Scilight

Advanced Characterization

https://www.sciltp.com/journals/ac

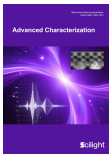

Review

Methods for Characterizing Adsorption on Solid Surfaces in Liquids

Charles T. Campbell [1,*] and Nirala Singh [2]

[1] Departments of Chemistry and Chemical Engineering, University of Washington, Seattle, WA 98195, USA
[2] Department of Chemical Engineering, University of Michigan, Ann Arbor, MI 48109, USA
* Correspondence: charliec@uw.edu

How To Cite: Campbell, C.T.; Singh, N. Methods for Characterizing Adsorption on Solid Surfaces in Liquids. *Advanced Characterization* **2026**, *1*(1), 84–97. https://doi.org/10.53941/ac.2026.100007

Received: 13 May 2026
Revised: 25 June 2026
Accepted: 25 June 2026
Published: 30 June 2026

Abstract: The recent surge in basic research studying liquid-phase surface reactions for catalytic biomass conversions and electrocatalytic reactions for energy storage and utilization highlights the importance of characterizing adsorbates at the liquid / solid interface and their surface chemical reactions. The design of new, more active, and selective catalysts for these reactions is vital. Typical catalytic reactions include multiple elementary steps involving many surface-bound intermediates and transition states. The energetics of these intermediates and transition states are crucial, as they determine the rate and selectivity of the catalysts. These energies are also essential to build accurate microkinetic models that predict activity and selectivity under different conditions and the few rate-controlling species whose energies can be tuned to make a better catalyst. Therefore, the ability to identify the adsorbed intermediates in catalytic reaction mechanisms and to predict the energies of these surface intermediates and their transition states for formation and further reaction are of critical importance. This is true for reactions at solid surfaces both in the gas phase and in liquids. We review here methods for studying adsorbates on solid surfaces in the liquid phase, their coverages, the rates of their formation and further surface reactions, the internal energies of these adsorbates, the activation free energies for their formation, and methods for estimating the effects of solvent choice and of interfacial electric fields on these adsorbate internal energies.

Keywords: adsorption at liquid/solid interfaces; solvent effects; adsorption kinetics; adsorbate energies; heterogeneous catalysis; electrocatalysis

1. Introduction

Liquid-phase catalytic and electrocatalytic reactions occurring at solid surfaces under liquids are becoming increasingly important for sustainable energy, environmental protection and other chemical industries. In typical catalytic reactions, there are many adsorbed intermediates and transition states in the elementary reaction steps that occur between reactants and products. Their energies are the key properties that determine the rate and selectivity of one solid catalyst compared to another [1–3]. These are the same energies that are required to build accurate microkinetic models of surface-catalyzed reactions [2–5]. This importance of adsorbed intermediates' energies is true for both gas-phase reactions and liquid-phase reactions occurring at the surface of solid catalyst materials, as well as for electrocatalytic reactions of all sorts. Therefore, to develop a fundamental understanding of how structural or compositional changes in catalyst materials (most particularly at their surfaces) affect catalytic reaction rates and selectivities, it is essential to know the identities of adsorbed catalytic reaction intermediates, their energies, and the activation energies for their formation and conversions to other species. We review here experimental methods for determining these crucial details of catalytic mechanisms for surfaces in liquid and electrochemical environments.

2. Structural Characterization of Liquid/Solid Interfaces

About 15 years ago, Zaera [6] reviewed methods that had been developed to probe adsorbates and the surface structure of liquid/solid interfaces. He discussed infrared absorption spectroscopy, one of the techniques most used for this purpose, and other vibrational spectroscopies, in particular Raman scattering spectroscopy and sum frequency generation. He discussed the use of UV-vis spectroscopies, employed mainly to obtain electronic information of adsorbates at the interface but also employed to quantify adsorbate coverages, and acoustic-based techniques such as quartz crystal microbalances, also used to measure coverages. He discussed the use of X-rays and neutrons, both in spectroscopic studies, to extract electronic information about the liquid/solid interface, and in scattering and diffraction modes, to acquire structural details of the interface. The potential use of techniques such as X-ray photoelectron spectroscopy and nuclear magnetic and electron spin resonance spectroscopies for characterization of liquid/solid interfaces was briefly surveyed. He also discussed approaches for acquisition of spatially resolved information on liquid/solid interfaces, including optical and scanning microscopies.

Many methods for characterizing liquid/solid interfaces were also discussed in an entire volume (#631, 2015) of the journal *Surface Science*, which was a special issue on "Surface Science and Electrochemistry". It covers predominantly the areas of in situ scanning tunnelling microscopy (STM) and electrochemical STM (EC-STM), other new experimental methods, underpotential deposition of epitaxial films, adsorption and self-organization of organic layers, model electrocatalysis, and new theoretical approaches.

Since Zaera's 2012 review and that 2015 special issue, many advances have been made in these techniques and new methods have been developed (see, for example, refs. [7–9]). Particularly important has been the evolution of methods for doing photoelectron spectroscopies at liquid/solid interfaces [10–14]. We will not go into further depth in reviewing these more general methods, but focus below on new experimental methods used to address the thermodynamics and kinetics of adsorption and adsorbate surface reactions in liquids as well as models for electric field and solvent effects on adsorbate energies.

3. Characterizing Adsorbate Coverages under Liquids

The earliest measurements of adsorbate coverage under liquids were simply from measuring the charge transferred upon the adsorption of ionic species from the liquid with electrochemical techniques. The adsorption of uncharged species is more challenging, but capacitance-type methods were developed very early to measure the potential dependence of adsorption of uncharged molecules [15,16]. Briefly, changes in the capacity of the double layer are used to understand adsorption coverages. These techniques derive from electrocapillary measurements, but with the added difficulty of operating with a solid electrode.

Radiotracer techniques were also used very early to probe adsorption amounts on different electrodes [17–19]. Here, an isotopically labeled organic compound is adsorbed and its radiation is measured and compared to bulk solution radiation to understand the surface concentration of the target species.

Thin-layer coulometry techniques were developed to determine adsorbate coverages via adsorption of species from a small volume of liquid and counting the charge associated with a later conversion reaction of that adsorbate or of the residue of its liquid-phase precursor [20–22]. Due to the low volumes, a distinction between electrochemical conversion of adsorbed species and non-adsorbed species was possible, and surface coverages on a solid electrode could be determined. These methods have been used to help distinguish adsorbates' molecular orientation, e.g., flat compared to edgewise.

Surface plasmon resonance (SPR) sensing has been used extensively to measure adsorption amounts versus time on solid surfaces in liquids. It is sensitive for adsorbates of moderate size, has ~1 s time resolution, and is easily calibrated for absolute coverage measurements [23–26]. Since SPR is so fast, it is particularly attractive for measuring adsorption kinetics [24,25]. It is widely used in biomolecular binding studies, like protein—ligand binding. It can be used in a highly parallel fashion via SPR microscopy to simultaneously measure thousands of on-rates, off-rates and/or equilibrium binding constants [27,28]. SPR is most widely used for surfaces with strong surface plasmon resonances like Au and Ag (sometimes coated with thin layers of other materials).

Electrochemical mass spectrometry (EC-MS) techniques like differential electrochemical mass spectrometry (DEMS), and online electrochemical mass spectrometry (OLEMS) have been developed that can probe the potential-dependent adsorption, desorption and reactions of species and quantify their coverages with submonolayer sensitivity and powerful species identification and differentiation [29–37].

One can also measure the coverage of adsorbed species by the extent to which they suppress peaks seen in cyclic voltammetry (CV) that are well-known to be due to chemistry on clean surface sites. For example, we measured the coverage of adsorbed phenol on platinum in aqueous solution using CV on Pt wires to assess the fractional coverage of adsorbed phenol as a function of the solution concentration of phenol. The fractional

coverage of phenol was estimated from the fractional suppression of the quantity of adsorbed H adatoms measured by the so-called H underpotential deposition (HUPD) peaks in CV, assuming competition for Pt sites and negligible effect of the post-adsorbed H on phenol adsorption amounts. Because the line shape and voltage of the HUPD CV peaks allows differentiation of the contributions of Pt(111) sites from lower-coordination sites (Pt(110)-like, Pt(100)-like, and step-edge sites) [38], we were able to separately determine the HUPD charges associated with Pt(111)-like terrace sites and lower-coordination Pt sites, and measure adsorption isotherms associated with both types of sites on the Pt wire [39]. The same approach can also be extended to other platinum group metals, such as Rh [40], but HUPD is limited in the metals to which it can be applied. Limitations of this HUPD CV technique include the possibility that the adsorbate has more complex interactions with co-adsorbed H than simple site blocking, and possible interferences from other co-adsorbates that limit the technique to use only in specific electrolyte solutions.

Adsorption amounts on metal surfaces in liquids have also been quantified by the charge associated with the adsorbate's displacement upon adsorption of CO. For example, specific adsorption of sulfate and phosphate anions on a Cu(100) electrode at pH 3 were quantified and studied in detail by the charge displacement measured upon the adsorption of CO [41].

4. Characterizing Adsorption and Desorption Kinetics in Liquids

Any of the above techniques that can measure adsorbate coverages with quantitative accuracy can be applied to measure coverage versus time during adsorption or desorption, whose slope gives the adsorption and/or desorption rate. An application of this is shown in Figure 1, where the coverage versus time measured using SPR with a time resolution below 1 s was used to calculate the adsorption rate of alkanethiols onto polycrystalline Au from ethanol solution at 300 K to make the corresponding adsorbed alkanethiolate [25].

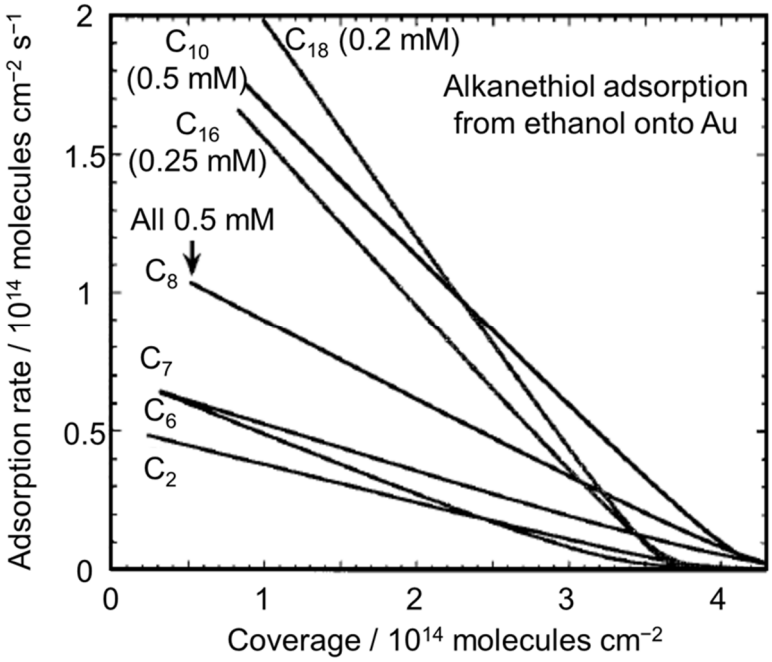

Figure 1. Adsorption rates versus coverage taken from the SPR response versus time upon adsorption of several linear alkanethiols (of different carbon chain lengths, C_n) from ethanol solution onto Au at room temperature. The adsorption transients were initiated by the injection of the alkanethiol solution of the following concentration into the SPR flow cell at time 0: C_2 (0.5 mM), C_6 (0.5 mM), C_7 (0.5 mM), C_8 (0.5 mM), C_{10} (0.5 mM), C_{12} (0.5 mM), C_{16} (0.25 mM), and C_{18} (0.2 mM). The rates were determined from the local derivative of the coverage versus time, after fitting to a triple exponential function. From Ref. [25], with permission. Copyright 2000, American Chemical Society.

These rates of adsorption were analyzed in detail to obtain from them the coverage-dependent sticking probability (S), which is the probability of adsorption per collision of alkanethiol solute molecule with the surface. These data were very well fitted with linear decrease in S with coverage (θ), as predicted by the first-order Langmuir adsorption mechanism [25]:

$$S = S_0 (1 - \theta/\theta_{max}), \quad (1)$$

where S_0 is the (extrapolated) initial sticking probability and θ/θ_{max} is the coverage relative to "maximum" coverage. "Maximum" coverage does not refer to true saturation, but to the extrapolation to zero of this best-fit linear decrease in sticking probability with coverage, which is ~20% below the true saturation for all the thiols (i.e., ~4.0×10^{14} versus ~4.8×10^{14} thiols/cm^2).

As shown in Figure 2, the resulting values of S_0 increased by a factor of ~65 with alkanethiol chain length, where the logarithm of S_0 is plotted versus chain length, N_{CH2}, defined as the number of methylene groups in the chain (not counting the terminal CH_3). The solid line shows the linear best fit to [25]:

$$S_0 = \upsilon \exp\left(\frac{E_0 - \left(0.65 \frac{kJ}{mol}\right) N_{CH2}}{RT}\right) \quad (2)$$

where E_0 is the activation free energy for methanethiol adsorption and υ is the prefactor. This best fit gave $\upsilon \exp[-(E_0/RT)] = 1.26 \times 10^{-8}$. This increase in S with N_{CH2} was attributed to the energetic effects of added methylene units on the stability (i.e., Gibb's free energy) of the transition state for adsorption (relative to the solution phase species). Within this picture, the slope corresponds to a decrease in the activation energy for adsorption by 0.65 kJ/mol per methylene group.

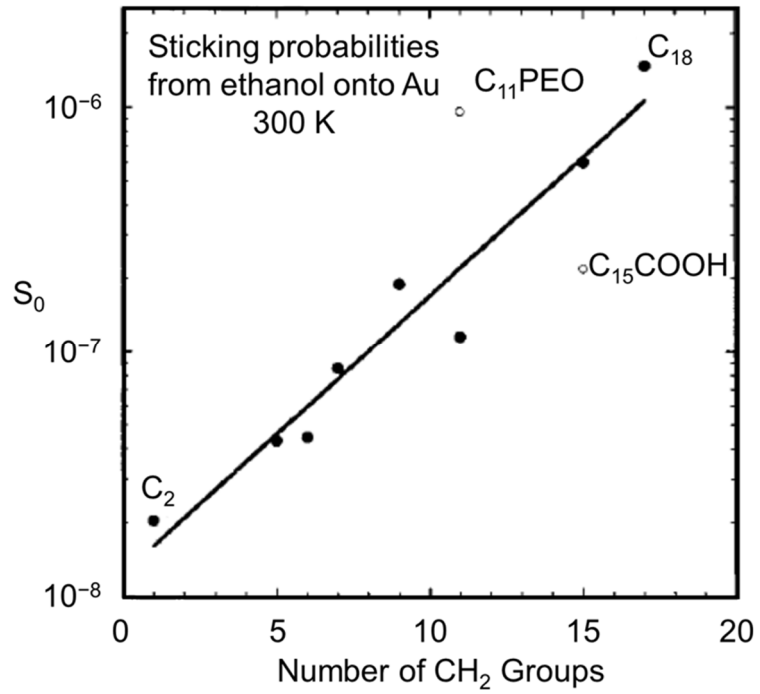

Figure 2. The initial sticking probability (S_0) plotted in log format versus chain length for alkanethiols (filled circles) adsorbing from ethanol solution onto Au at 298 K. The open circles show S_0 for the C_{11}PEO and C_{15}COOH thiols. The solid line shows the linear best fit to the data for the simple alkanethiols (filled circles), which corresponds to Equation (2). From Ref. [25] with permission. Copyright 2000, American Chemical Society.

Just the opposite trend was seen in the reverse (desorption) rates of these same thiolate species by Bain et al. [42], who reported that their activation energy for desorption into hexadecane solvent increases by ~0.8 kJ/mol per methylene group. They postulated that this arises from stabilization of the adsorbed state due to additional attractive interactions to the surface (and the other thiols there) with each added methylene group. Combining these results, a fairly complete picture of the free-energy surface for the adsorption / desorption process evolved [25]: Summing the effects of chain length on the adsorption and desorption activation free energies (−0.65 and +0.8 kJ/mol per methylene, respectively), we estimated that the adsorbed state is stabilized by ~1.5 kJ/mol per methylene group [25]. Thus, the adsorption rates of alkanethiols on Au in ethanol show a linear free energy (or BEP) relationship with a transition state energy that varies linearly with changes in the net reaction energy with a slope (β) of 0.45. Using this and other literature, we estimated the absolute free energy of adsorption to be about 30 kJ/mol downhill for propanethiol [25] and more downhill for the longer alkanethiols by ~1.5 kJ/mol per methylene group. Assuming that the prefactor for the sticking probability of adsorption, υ, is unity gave that $E_0 = 45$ kJ/mol, so that the free energies for the transition state for adsorption of the C_2 and C_{18} thiols were 43 and

33 kJ/mol higher than that for the same alkanethiol in solution [25]. In ultrahigh vacuum, these thiols have near unit sticking probability on clean Au surfaces, and thus nearly negligible activation barriers. We attributed these much larger activation barriers seen in liquid ethanol to the energy cost to displace adsorbed solvent molecule(s) from the gold, and the loss of solvent molecules from the solvation shell of the dissolved thiol. This energy cost to displace adsorbed solvent molecules from the surface also shows up as a decrease in the heat of adsorption due to the solvent, as discussed in detail below. A calorimetry study of COOH-terminated C_2-C_5 alkythiol adsorption from water onto Au at 298 K showed it to be downhill in free energy by ~38 kJ/mol [43], similar to the estimates above for alkanethiols on Au in ethanol.

If one repeated the above types of measurements of rates of adsorption (or desorption) at various temperatures, one could extract the apparent activation energy and activation entropy for adsorption (or desorption) more directly than done in the example above.

5. Characterizing Adsorption Thermodynamics in Liquids: Heats and Entropies of Adsorption

Any of the above methods for measuring adsorbate coverages in liquids can also be applied to determine the equilibrium coverage versus solute concentration at fixed temperature and, from this, the equilibrium constant for adsorption, K_{eq}. For an example, see ref [39]. This also provides the standard-state free energy of adsorption, $\Delta G_{ads}^0 = -RT \ln(K_{eq})$. Repeating this at different temperatures allows for analysis with the Van't Hoff equation to obtain the standard enthalpy of adsorption, ΔH_{ads}^0. Since the standard entropy of adsorption, ΔS_{ads}^0, can be estimated for many systems based on experimental trends [44,45], the value of ΔG_{ads}^0 at one temperature can even allow for a good estimate of $\Delta H_{ads}^0 = \Delta G_{ads}^0 + T\,\Delta S_{ads}^0$ (see, for example, refs. [39,46]).

Adsorption calorimetry can also be performed using commercial isothermal titration calorimeters (ITCs) to directly measure heats of adsorption from liquid solutions onto catalyst powders dispersed in solvent [43,47–49]. The sensitivity is very high for such adsorption calorimeters (with a standard deviation of ±1.5 kJ/mol). However, the surfaces of such powders are usually rather poorly defined, unless powders are used that are specially prepared to expose mainly only one or a few well-defined surface facets. This type of adsorption calorimetry has recently been extended to allow in situ measurement of catalyst open circuit potentials (E_{cat}) under the same conditions [50]. This gives access to other important thermodynamic quantities relevant to electrocatalysis and electric field effects in thermal catalysis in liquids.

Schuster's group has developed an adsorption calorimeter for measuring the heat effect of electrochemical reactions occurring at flat electrode surfaces, including single crystalline metal surfaces like Au(111) [51–56]. It employs a PVDF pyroelectric heat detector, similar to that developed by Campbell's group for measuring heats of adsorption of gas-phase species on single crystals. In Schuster's approach, the measured heat, which is reversibly exchanged at a single electrode, directly correlates with the entropy change during the electrochemical reaction. Since the electrode potential gives the reaction free energy, this measured entropy allows one to determine the enthalpy change as well. With their experimental improvements, surface electrochemical reactions with tiny submonolayer conversion have become accessible for heat measurements [51].

6. Estimating Liquid Solvent Effects on Adsorption Energies

Predicting the internal energies of adsorbed reaction intermediates on solid surfaces in liquid solvents is important for improving catalytic and electrocatalytic reactions such as those used in the production of fuels, fuel cells, biomass conversions, methane and CO_2 conversions, plastics upcycling, and environmental remediation. The increasing importance of these reactions on solid surfaces *in liquid phase* highlights the need for an improved basic understanding of how solvents affect adsorption. The choice of solvent is well known to strongly influence catalytic activity and selectivity [57–68]. The reasons for this are still not well understood, but certainly derive mainly from the effects of the solvents on the energies of adsorbed reaction intermediates and elementary-step transition states.

Due to the vast knowledge of reaction energies at gas/solid interfaces and methods for studying them compared to liquid/solid interfaces, it would be extremely valuable to learn how to transfer current knowledge of the energetics of reactions at gas/solid interfaces to liquid/solid interfaces. Particularly important is the development of methods for estimating the effect of liquid solvents on the internal energies of adsorbed reaction intermediates and transition states in catalytic and electrocatalytic reaction mechanisms. This would facilitate development of microkinetic models for estimating reaction kinetics in solution, which has proven extremely useful in gas-phase catalysis research [2–5,45,69–92]. In cases where adsorption energies in liquids have been measured, the solvents have had large effects, as illustrated in Figure 3, which compares phenol on Pt(111) in water versus gas phase.

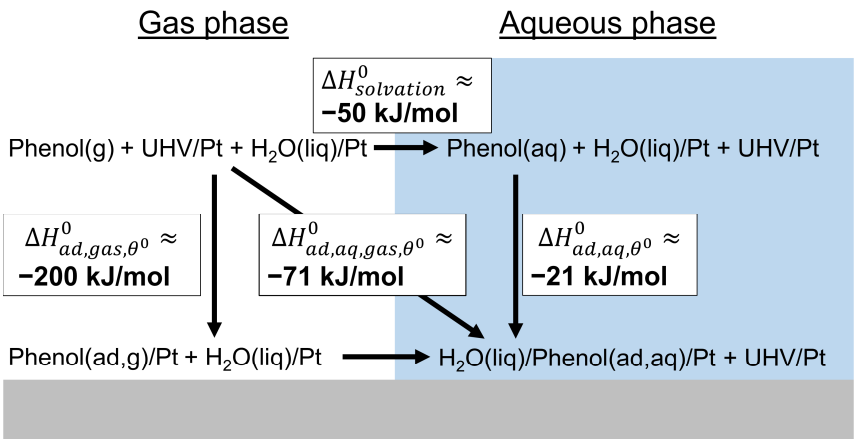

Figure 3. Thermodynamic cycle comparing experimental phenol adsorption enthalpies in gas and aqueous phases on a Pt(111) surface, where UHV/Pt refers to ultrahigh vacuum above the clean Pt surface. From Ref. [39], with permission. Copyright 2019, American Chemical Society.

There have been numerous other studies to compare heats of adsorption measured in liquid solvents with those in the gas phase [40,46,93–98] and to use simulations to clarify the role of the solvent [57,59,68,94,96,99,100]. Additionally, there are several reviews and viewpoints that discuss the challenges involved in modeling solvent effects [101,102]. Generally, modeling efforts to computationally incorporate solvent effects in studying surface chemical reactions include: implicit modeling of the solvent as a homogeneous constant dielectric continuum, bilayer adsorption (ice model), explicit modeling of the solvent by inclusion of solvent molecules in the simulation, mixtures of implicit and explicit solvation, QM/MM approaches, and ab-initio-MD simulations [101–119]. These models have successfully illustrated the importance of including co-adsorbates, solvents, and electric fields in theoretical models.

Singh and Campbell [46] developed a simple "interfacial bond-additivity" model to estimate the energies of neutral adsorbates on solid surfaces in the liquid phase using measured gas phase adsorption energies and the adhesion energy of the solvent to the solid. They recently extended that model, initially derived for planar molecules (e.g., phenol), to adsorbates of finite thickness and arbitrary shape [97]. Their model allows one to estimate the internal energy change upon adsorption of a reactant R from liquid solvent ($\Delta U_{ads,R(solvent)}$) based on six values that are known or can be measured or estimated with reasonable accuracy: (1) the molecule's gas-phase adsorption energy on the surface, as might be measured in vacuum experiments ($\Delta U_{ads,R(gas)}$), (2) the adhesion (internal) energy per unit area of the solvent to the bare solid surface ($E_{adh,S/M}$), (3) the surface area where solvent molecules are blocked by the adsorbate (σ_R), (4) the total "surface area" of the solvent cavity that must be created to solvate the free reactant molecule (σ_{tot}), (5) the reactant's solvation energy (relative to the free gas-phase molecule) per mole ($\Delta U_{solvation,R(gas)}$), and (6) the liquid solvent's surface internal energy ($\gamma_{S(liq)}$) [97]:

$$\Delta U_{ads,R(solvent)} = \Delta U_{ads,R(gas)} + \left[E_{adh,S/M} - \frac{\Delta U_{solvation,R(gas)}}{\sigma_{tot}} - \gamma_{S(liq)}\right]\sigma_R \quad (3)$$

The first three of these parameters can be measured, the sixth is known for many liquids, the fifth can be derived from the temperature dependence of the reactant's Henry's law constant in that liquid, and the fourth can be estimated from the volume of the adsorbate molecule in its liquid form and its approximate shape.

This equation only applies to charge-neutral molecules. By studying these values for several systems, they found that the adsorption energy in the solvent is smaller in magnitude than in the gas phase by approximately the adhesion energy of the solvent to the solid times the surface area from which solvent molecules are displaced upon reactant adsorption. Of the three terms in the bracket on the right side of this equation, they found that the last two are of opposite sign and often close in magnitude, so they nearly cancel. Singh and Campbell found values for these two terms for many molecules and four solvents, and showed that they differed by ~20 kJ/mol at most [46,97], which is non-negligible but still very small compared to the $E_{adh,S/M}$ term, so that:

$$\Delta U_{ads,R(solvent)} = \Delta U_{ads,R(gas)} + \sigma_R E_{adh,S/M} + \text{small terms.} \quad (4)$$

Clearly, solvent/metal adhesion energies are crucial in predicting adsorption energies in solvents based on gas-phase adsorption energies and thus in understanding the effects of different solvents on adsorption energetics and catalysis. Note that the footprint area of the adsorbate per mole, σ_R, can be determined from the experimentally measured saturation (closest-packed) coverage of the adsorbate in the first layer in UHV [46,97].

The known molar volume of the reactant molecule (V_m, calculated from its reported density as a pure bulk liquid), when divided by this footprint area, gives an estimate of the molecule's thickness, $t = V_m/\sigma_R$. One can then estimate σ_{tot} for the adsorbate using this thickness and footprint area, by assuming some approximate shape of the adsorbate (e.g., cylindrical disk, rod, etc.) [97].

The derivation of Equation (3) made two bond-additivity-like approximations that certainly have some errors:

1. The bond energy of the adsorbate to the surface and its orientation are not affected by the presence of solvent molecules contacting the *other* sides of the adsorbate (compared to the other sides of the adsorbate contacting vacuum).
2. The bond energy of the solvent to the adsorbate, per unit area of solvent-adsorbate contact, is not affected by the presence of the solid surface bonding to the *other* side of the adsorbate (compared to solvent being there instead of the solid surface, i.e., when the adsorbate is fully surrounded by solvent instead).

By comparing the predictions of this model to measured adsorption (internal) energies in solvents [40,97,98,120] and to simulations [112] the model was found to be reasonably accurate, capturing most of the difference between the adsorption energy in the solvent compared to that in the gas phase, but not all of it. For example, the measured adsorption energy of phenol on Pt(111) is 174 kJ/mol in UHV, but only 19 kJ/mol in water, and the model captures 67% (or 104 kJ/mol) of this large difference (155 kJ/mol) [97]. The model captures most of the solvent effects on adsorption energies and therefore opens many opportunities for predicting adsorption energies in solutions in a semi-quantitative way. Those predictions can be leveraged to qualitatively predict solvent effects on catalytic reaction rates. For example, solvent tuning was used to control the coverage of formate and thus control the rate of Pd-catalyzed transfer hydrogenation [121].

Clearly, to use this model requires knowing the adhesion energies per unit area of the liquid solvents to the catalyst and electrocatalyst surfaces of interest. We have made experimental measurements to estimate the adhesion energies for many solvent / solid surface combinations [122,123].

As noted above, we estimated the absolute free energy of adsorption of propanethiol from ethanol solution onto Au (to make adsorbed propanethiolate) to be about 30 kJ/mol downhill, and estimated that, for longer-chain alkanethiols, this adsorbate is stabilized by ~1.5 kJ/mol per methylene group (relative to the corresponding solution-phase thiol) [25]. We also found that the transition state for adsorption of these C_2 and C_{18} thiols were 43 and 33 kJ/mol higher, respectively, than that for the same alkanethiol in bulk solution [25], whereas these thiols have negligible activation barriers to adsorb in ultrahigh vacuum (in the absence of the liquid ethanol). We attributed this large difference mainly to the energy cost to displace adsorbed solvent molecule(s) from the gold. According to Equation (4), this energy cost to displace adsorbed solvent molecules from the surface should also manifest itself as a substantial decrease in the heat of adsorption due to the solvent. This highlights the close connection between thermodynamics of adsorption in liquids and their kinetics.

Let us assume that the adhesion energy of ethanol to Au is about 0.13 J/m^2, since E_{adh} for both methanol and n-hexane to Pt(111) is ~0.16 J/m^2 [123]. Inverting the full coverage of 4×10^{14} thiols/cm^2 (θ_{max} from above) gives the area per thiol. The product of these two (after units conversion) equals 20 kJ/mol. Thus, Equation (4) predicts that alkanethiol adsorption on Au in ethanol liquid should be about 20 kJ/mol less exothermic than in vacuum. This is similar in magnitude to the destabilization of the transition state for adsorption of these C_2 and C_{18} thiols due to liquid ethanol of 43 and 33 kJ/mol estimated from the sticking probabilities (see above).

The method of Equation (3) is very approximate, and that of Equation (4) is even less accurate. Nevertheless, they could be very useful in estimating the effects of changing solvent on the energies of adsorbed catalytic intermediates. Such estimates could provide important new ideas for improving catalytic and electrocatalytic processes in the liquid phase through tuning the solvent and its composition.

7. Effects of Electric Fields on the Energies of Adsorbates on Metal Surfaces in Liquids

As noted above, understanding how liquid solvents affect the energies of adsorbed catalytic reaction intermediates, compared to their much better-known values in gas phase, is crucial for understanding both liquid-phase heterogeneous catalysis and electrocatalysis. There has been recently-growing proof that thermochemical catalysis on metals in liquids can proceed via the electrochemical coupling of two complementary electrochemical half-reactions with equal and opposite electron stoichiometry, especially based on results from the groups of Surendranath, Román, Flaherty and Baiker [124–133]. These studies have shown that metal catalysts undergo spontaneous electrical polarization during thermal catalysis in liquid phase, and that the electrochemical potential of the catalyst is a critical determinant of reaction rate and selectivity. They also developed methods for measuring this polarization.

The above results prove that, when doing either thermal catalysis in liquids like water or purposeful electrocatalysis on metal surfaces, one *must* consider that there is an electrical double layer near the metal surface across which there is a large change in electrostatic potential and therefore a large electric field. Changes in that electric field will certainly affect the energies of adsorbed catalytic reaction intermediates and transition states on the metal surface, and these energies are crucial in determining reaction rates. Knowing how changes in this electric field affect the energies of adsorbed reaction intermediates and transition states is therefore a crucially important part of understanding how liquid solvents affect adsorbate (and transition state) energies.

We recently reviewed what is known regarding the effects of electric fields on the energies of adsorbed catalytic reaction intermediates on metal surfaces in both liquid solvents and in ultrahigh vacuum (UHV) [134]. That review focused on what was learned about this from surface science studies performed in UHV, and showed how that can guide predictions about how changes in electric fields in the nearby double layer affect adsorbate energies on metal surfaces in liquids. In UHV, the electric field felt by an adsorbate can be strongly tuned by the addition of a different adsorbed species nearby. Alkali adatoms exert a very strong change in electric field near the metal surface, as quantified by work function measurements. The effects of these changes in field due to alkali adatoms on the energies of co-adsorbed catalytic reaction intermediates, their electronic character and their reaction rates have been studied extensively for decades on clean, well-ordered single-crystal metal surfaces in UHV. For example, their field stabilizes adsorbed CO, N_2, and H, weakens their C-O and N-N bonds and increases the dissociation rates of adsorbed CO and N_2. These studies provide insight into the effects of applied electric fields on neutral and relatively non-polar adsorbates in liquid environments, if we assume that changes in the field have only small effects on the strength of the weak attractions between adsorbate and solvent, so that the change in adsorbate energy with a change in its local electric field is the same change as when adsorbed in UHV. For example, this approach explains the well-known observation that the binding energy of hydrogen adatoms (H_{ad}) to many late transition metal surfaces, as probed by cyclic voltammetry in aqueous solutions, increases (bind more strongly) with increasing pH, as shown in Figure 4. This change in H_{ad} energy in turn explains pH-induced changes observed in the rates of many aqueous-phase thermal catalytic and electrocatalytic hydrogenation reactions in which H_{ad} must add to another species, as shown by example for one thermal catalytic reaction (phenol hydrogenation over Pt) in Figure 4.

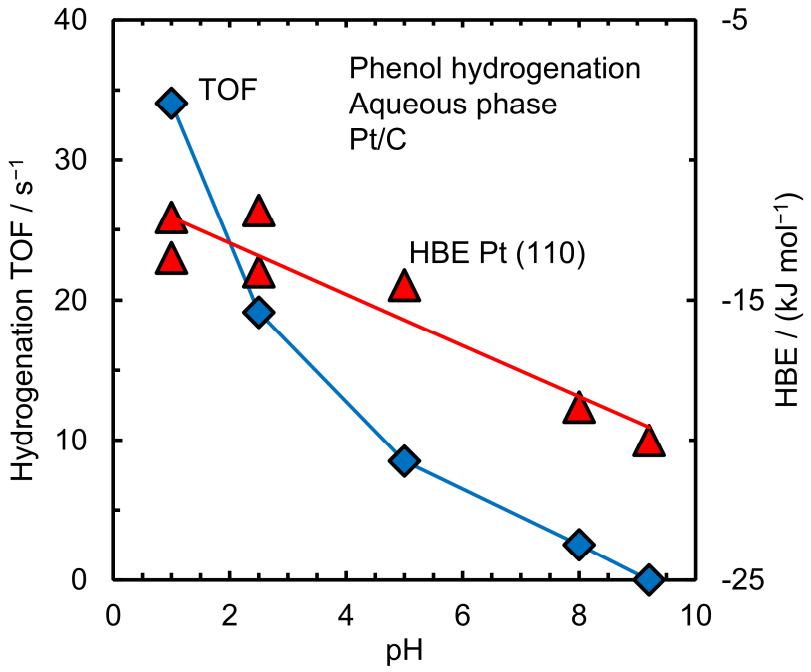

Figure 4. Initial rates per Pt surface atom (TOF, in blue) for aqueous-phase phenol hydrogenation over 5 wt % Pt on carbon at 353 K at 20 bar H_2 versus pH. Also shown (in red) is the hydrogen adatom binding energy to Pt(110) versus pH, measured in aqueous phase by Sheng et al. using CV [135]. Reproduced from Ref. [100]. Copyright 2019, American Chemical Society.

This effect of electric field on the energy of H_{ad} and its reactivity is just for one example adsorbate. Our recent review [134] summarizes how the interfacial electric field affects many other uncharged adsorbates and even some of their reactive transition states in UHV. It goes on to suggest how those results in UHV can guide predictions

about how this electric field will affect these same adsorbates at the liquid/metal interface. It also summarizes what is known about field effects on adsorbate energies from in situ liquid-phase and electrochemical studies.

Clearly, being able to predict the effects of electric fields on adsorbate energies has important practical implications for electrocatalytic and even thermal catalytic reactions, opening up the possibilities for tuning reaction rates and selectivities via modulation of the electric field near the surface by variations in applied potential or solute concentrations (e.g., pH, alkali ions, etc.).

A very important advance to help probe electric field effects in liquid-phase electrocatalysis and thermal catalysis has been the use of infrared Stark tuning measurements of adsorbed CO to probe the field near the metal surface. For example, Resasco's group [136] recently demonstrated that organic alkylammonium cations influence electrocatalytic rates of CO_2 reduction over Ag in non-aqueous media in an alkyl chain-length dependent way consistent with the strength of the electric field at the catalyst surface, determined by Stark tuning measurements of adsorbed CO on Pt with these same cations and solvent. They attributed the observed rate changes to field-induced changes in the energy of the adsorbed CO_2. Exceptionally important for probing these effects in thermal catalysis was the recent development of methods for wirelessly monitoring and controlling spontaneous electrical polarization at conductive catalysts dispersed in liquids employing infrared Stark spectroscopy by Wesley, Román, and Surendranath [127]. They used this to effectively track the magnitude of interfacial polarization at distributed metal/liquid interfaces at many different reaction conditions.

8. Concluding Remarks

Many methods are now available for studying adsorbates on solid surfaces in the liquid phase, their coverages, the rates of their formation and further surface reactions, their adsorption energies, methods for estimating the effects of solvent on these adsorption energies, and the effects of interfacial electric fields on these adsorbate energies. However, compared to adsorbates on solids in gas phase, these methods are much more limited and challenging to perform. This highlights the importance of developing new methods to study liquid/solid interfaces, and for combining theory with experiments to better understand such interfaces. New methods to study liquid/solid interfaces that leverage what has been learned at the gas/solid interface and what can be measured at the gas/solid interface appear particularly promising for the near future.

Author Contributions

Both authors made substantial contributions to the conception or design of the paper. C.T.C. drafted the paper and N.S. substantively revised it. All authors have read and agreed to the published version of the manuscript.

Funding

C.T.C. gratefully acknowledges the financial support for this work by the National Science Foundation under Grants #CBET-2415041 and #CBET-2415040, and by the B. Seymour Rabinovitch Chair Endowment. N.S. acknowledges National Science Foundation Grant 2236770.

Conflicts of Interest

The authors declare no conflict of interest.

Use of AI and AI-Assisted Technologies

No AI tools were utilized for this paper.

References

1. Ertl, G. Reactions at Surfaces: From Atoms to Complexity (Nobel Lecture). *Angew. Chemie. Int. Ed.* **2008**, *47*, 2–14.
2. Dumesic, J.A.; Huber, G.W.; et al. Microkinetics. In *Handbook of Heterogeneous Catalysis*, 2nd ed.; Ertl, G., Knözinger, H.; Schüth, F., et al, Eds.; Wiley-VCH Gmbh: Weinheim, Germany, 2008; pp. 1445–1462.
3. Campbell, C.T. The Degree of Rate Control: A Powerful Tool for Catalysis Research. *ACS Catal.* **2017**, *7*, 2770–2779.
4. Norskov, J.K.; Bligaard, T.; Rossmeisl, J.; et al. Towards the computational design of solid catalysts. *Nat. Chem.* **2009**, *1*, 37–46.
5. Nørskov, J.K.; Abild-Pedersen, F.; Studt, F.; et al. Density functional theory in surface chemistry and catalysis. *Proc. Natl. Acad. Sci. USA* **2011**, *108*, 937–943.
6. Zaera, F. Probing Liquid/Solid Interfaces at the Molecular Level. *Chem. Rev.* **2012**, *112*, 2920–2986.

7. Auer, A.; Eder, B.; Giessibl, F.J. Electrochemical AFM/STM with a qPlus sensor: A versatile tool to study solid-liquid interfaces. *J. Chem. Phys.* **2023**, *159*, 174201.
8. Pastor, E.; Lian, Z.; Xia, L.; et al. Complementary probes for the electrochemical interface. *Nat. Rev. Chem.* **2024**, *8*, 159–178.
9. Johannsmann, D.; Reviakine, I. Quartz crystal microbalance with dissipation monitoring for studying soft matter at interfaces. *Nat. Rev. Methods Primers* **2024**, *4*, 63.
10. Brummel, O.; Lykhach, Y.; Ralaiarisoa, M.; et al. A Versatile Approach to Electrochemical In Situ Ambient-Pressure X-ray Photoelectron Spectroscopy: Application to a Complex Model Catalyst. *J. Phys. Chem. Lett.* **2022**, *13*, 11015–11022.
11. Starr, D.E.; Favaro, M.; Abdi, F.F.; et al. Combined soft and hard X-ray ambient pressure photoelectron spectroscopy studies of semiconductor/electrolyte interfaces. *J. Electron Spectrosc. Relat. Phenom.* **2017**, *221*, 106–115.
12. Stoerzinger, K.A.; Hong, W.T.; Crumlin, E.J.; et al. Insights into Electrochemical Reactions from Ambient Pressure Photoelectron Spectroscopy. *Acc. Chem. Res.* **2015**, *48*, 2976–2983.
13. Yang, Y.; Feijóo, J.; Briega-Martos, V.; et al. Operando methods: A new era of electrochemistry. *Curr. Opin. Electrochem.* **2023**, *42*, 101403.
14. Zang, Y.J.; Shi, S.C.; Liu, J.; et al. Direct Probing the Electrical Double Layer at Graphite/Nafion Interface via Depth Profiling APXPS. *J. Am. Chem. Soc.* **2025**, *147*, 33366–33371.
15. Gileadi, E.; Rubin, B.R.; Bockris, J.O.M. Electrosorption of Ethylene on Platinum as a Function of Potential Concentration and Temperature. *J. Phys. Chem.* **1965**, *69*, 3335–3345.
16. Gileadi, E. Electrosorption of Uncharged Molecules on Solid Electrodes. *J. Electroanal. Chem.* **1966**, *11*, 137–151.
17. Gileadi, E.; Duic, L.; Bockris, J.O. A Comparison of Radiotracer and Electrochemical Methods for Measurement of Electrosorption of Organic Molecules. *Electrochim. Acta* **1968**, *13*, 1915–1935.
18. Heiland, W.; Gileadi, E.; Bockris, J.O. Kineitc and Thermodynamic Aspects of Electrosorption of Benzene on Platinim Electrodes. *J. Phys. Chem.* **1966**, *70*, 1207–1216.
19. Corrigan, D.S.; Krauskopf, E.K.; Rice, L.M.; et al. Adsorption of Acetic-Acid at Platinum and Gold Electrodes—A Combined Infrared Spectroscopic And Radiotracer Study. *J. Phys. Chem.* **1988**, *92*, 1596–1601.
20. Chia, V.K.F.; Soriaga, M.P.; Hubbard, A.T. The Adsorption, Orientation and Electrochemical Oxidation of Hydroquinone At Smooth Platinum-Electrodes—The Effect Of Electrode Potential. *J. Electroanal. Chem.* **1984**, *167*, 97–106.
21. Soriaga, M.P.; White, J.H.; Hubbard, A.T. Orientation of Aromatic-Compounds Adsorbed on Platinum-Electrodes—The Effect of Temperature. *J. Phys. Chem.* **1983**, *87*, 3048–3054.
22. Soriaga, M.P.; Hubbard, A.T. Determination of The Orientation of Adsorbed Molecules at Solid-Liquid Interfaces by Thin-Layer Electrochemistry—Aromatic-Compounds at Platinum-Electrodes. *J. Am. Chem. Soc.* **1982**, *104*, 2735–2742.
23. Jung, L.S.; Campbell, C.T.; Chinowsky, T.M.; et al. Quantitative Interpretation of the Response of Surface Plasmon Resonance Sensors to Adsorbed Films. *Langmuir* **1998**, *14*, 5636–5648.
24. Jung, L.S.; Campbell, C.T. Sticking probabilities in adsorption from liquid solutions: Alkylthiols on gold. *Phys. Rev. Lett.* **2000**, *84*, 5164–5167.
25. Jung, L.S.; Campbell, C.T. Sticking probabilities in adsorption of alkanethiols from liquid ethanol solution onto gold. *J. Phys. Chem. B* **2000**, *104*, 11168–11178.
26. Jung, L.S.; Nelson, K.E.; Stayton, P.S.; et al. Binding and dissociation kinetics of wild-type and mutant streptavidins on mixed biotin-containing alkylthiolate monolayers. *Langmuir* **2000**, *16*, 9421–9432.
27. Shumaker-Parry, J.S.; Campbell, C.T. Quantitative methods for spatially resolved adsorption/desorption measurements in real time by surface plasmon resonance microscopy. *Anal. Chem.* **2004**, *76*, 907–917.
28. Campbell, C.T.; Kim, G. SPR microscopy and its applications to high-throughput analyses of biomolecular binding events and their kinetics. *Biomaterials* **2007**, *28*, 2380–2392.
29. Hartung, T.; Baltruschat, H. Differential Electrochemical Mass-Spectrometry Using Smooth Electrodes—Adsorption And H/D-Exchange Reactions of Benzene on pt. *Langmuir* **1990**, *6*, 953–957.
30. Baltruschat, H. Differential electrochemical mass spectrometry. *J. Am. Soc. Mass Spectrom.* **2004**, *15*, 1693–1706.
31. Bakshi, H.B.; Lucky, C.; Chen, H.S.; et al. Electrocatalytic Scission of Unactivated C(sp3)-C(sp3) Bonds through Real-Time Manipulation of Surface-Bound Intermediates. *J. Am. Chem. Soc.* **2023**, *145*, 13742–13749.
32. Lucky, C.; Fuller, L.; Schreier, M. Determining the potential-dependent identity of methane adsorbates at Pt electrodes using EC-MS. *Catal. Sci. Technol.* **2024**, *14*, 353–361.
33. Huang, J.H.; Scott, S.B.; Chorkendorff, I.; et al. Online Electrochemistry-Mass Spectrometry Evaluation of the Acidic Oxygen Evolution Reaction at Supported Catalysts. *Acs Catal.* **2021**, *11*, 12745–12753.
34. Krempl, K.; Hochfilzer, D.; Scott, S.B.; et al. Dynamic Interfacial Reaction Rates from Electrochemistry-Mass Spectrometry. *Anal. Chem.* **2021**, *93*, 7022–7028.

35. Trimarco, D.B.; Scott, S.B.; Thilsted, A.H.; et al. Enabling real-time detection of electrochemical desorption phenomena with sub-monolayer sensitivity. *Electrochim. Acta* **2018**, *268*, 520–530.
36. Winiwarter, A.; Boyd, M.J.; Scott, S.B.; et al. CO as a Probe Molecule to Study Surface Adsorbates during Electrochemical Oxidation of Propene. *Chemelectrochem* **2021**, *8*, 250–256.
37. Bhadouria, A.; Heil, J.N.; Parab, D.E.; et al. Propane Activation on Pt Electrodes at Room Temperature: Quantification of Adsorbate Identity and Coverage. *Angew. Chem. Int. Ed.* **2025**, *64*, e202421613.
38. McCrum, I.T.; Janik, M.J. Deconvoluting Cyclic Voltammograms To Accurately Calculate Pt Electrochemically Active Surface Area. *J. Phys. Chem. C* **2017**, *121*, 6237–6245.
39. Singh, N.; Sanyal, U.; Fulton, J.L.; et al. Quantifying adsorption of organic molecules on platinum in aqueous phase by hydrogen site blocking and in situ X-ray absorption spectroscopy. *ACS Catal.* **2019**, *9*, 6869–6881.
40. Akinola, J.; Barth, I.; Goldsmith, B.R.; et al. Adsorption Energies of Oxygenated Aromatics and Organics on Rhodium and Platinum in Aqueous Phase. *ACS Catal.* **2020**, *10*, 4929–4941.
41. Koga, O.; Watanabe, Y.; Tanizaki, M.; et al. Specific adsorption of anions on a copper (100) single crystal electrode studied by charge displacement by CO adsorption and infrared spectroscopy. *Electrochim. Acta* **2001**, *46*, 3083–3090.
42. Bain, C.D.; Troughton, E.B.; Tao, Y.T.; et al. Formation of Monolayer Films by The Spontaneous Assembly of Organic Thiols From Solution Onto Gold. *J. Am. Chem. Soc.* **1989**, *111*, 321–335.
43. Ravi, V.; Binz, J.M.; Rioux, R.M. Thermodynamic Profiles at the Solvated Inorganic-Organic Interface: The Case of Gold-Thiolate Monolayers. *Nano Lett.* **2013**, *13*, 4442–4448.
44. Campbell, C.T.; Sellers, J.R.V. The Entropies of Adsorbed Molecules. *J. Am. Chem. Soc.* **2012**, *134*, 18109–18115.
45. Campbell, C.T.; Sprowl, L.H.; Arnadottir, L. Equilibrium Constants and Rate Constants for Adsorbates: Two-Dimensional (2D) Ideal Gas, 2D Ideal Lattice Gas, and Ideal Hindered Translator Models. *J. Phys. Chem. C* **2016**, *120*, 10283–10297.
46. Singh, N.; Campbell, C.T. A Simple Bond-Additivity Model Explains Large Decreases in Heats of Adsorption in Solvents Versus Gas Phase: A Case Study with Phenol on Pt(111) in Water. *ACS Catal.* **2019**, *9*, 8116–8127.
47. Goobes, R.; Goobes, G.; Shaw, W.J.; et al. Thermodynamic roles of basic amino acids in statherin recognition of hydroxyapatite. *Biochemistry* **2007**, *46*, 4725–4733.
48. Crowe, M.C.; Campbell, C.T. Adsorption Microcalorimetry: Recent Advances in Instrumentation and Application. *Annu. Rev. Anal. Chem.* **2011**, *4*, 41–58.
49. Song, Y.; Sanyal, U.; Pangotra, D.; et al. Hydrogenation of benzaldehyde via electrocatalysis and thermal catalysis on carbon-supported metals. *J. Catal.* **2018**, *359*, 68–75.
50. Broomhead, W.T.; Flaherty, D.W. Microcalorimetric quantification of hydrogen adsorption thermodynamics in water-solvated systems on Pt/C. *Faraday Discuss.* **2026**. https://doi.org/10.1039/D5FD00170F Available online: https://pubs.rsc.org/en/content/articlelanding/2026/fd/d5fd00170f/unauth (accessed on 30 May 2026).
51. Schuster, R. Electrochemical microcalorimetry at single electrodes. *Curr. Opin. Electrochem.* **2017**, *1*, 88–94.
52. Etzel, K.D.; Bickel, K.R.; Schuster, R. Heat Effects upon Electrochemical Copper Deposition on Polycrystalline Gold. *Chemphyschem* **2010**, *11*, 1416–1424.
53. Bickel, K.R.; Etzel, K.D.; Halka, V.; et al. Microcalorimetric determination of heat changes caused by overpotential upon electrochemical Ag bulk deposition. *Electrochim. Acta* **2013**, *112*, 801–812.
54. Gottfried, J.M.; Schuster, R. Surface Microcalorimetry. In *Surface and Interface Science*; Wandelt, K., Ed.; Wiley-VCH: Weinheim, Germany, 2014.
55. Frittmann, S.; Halka, V.; Schuster, R. Identification of Non-Faradaic Processes by Measurement of the Electrochemical Peltier Heat during the Silver Underpotential Deposition on Au(111). *Angew. Chem. Int. Ed.* **2016**, *55*, 4688–4691.
56. Schönig, M.; Frittmann, S.; Schuster, R. Identification of Electrochemically Adsorbed Species via Electrochemical Microcalorimetry: Sulfate Adsorption on Au(111). *Chemphyschem* **2022**, *23*, e202200227.
57. Walker, T.W.; Chew, A.K.; Li, H.X.; et al. Universal kinetic solvent effects in acid-catalyzed reactions of biomass-derived oxygenates. *Energy Environ. Sci.* **2018**, *11*, 617–628.
58. Mellmer, M.A.; Sener, C.; Gallo, J.M.R.; et al. Solvent Effects in Acid-Catalyzed Biomass Conversion Reactions. *Angew. Chem. Int. Ed.* **2014**, *53*, 11872–11875.
59. Mellmer, M.A.; Sanpitakseree, C.; Demir, B.; et al. Solvent-enabled control of reactivity for liquid-phase reactions of biomass-derived compounds. *Nat. Catal.* **2018**, *1*, 199–207.
60. Gonzo, E.E.; Boudart, M. Catalytic-Hydrogenation of Cyclohexene: 3. Gas-Phase and Liquid-Phase Reaction On Supported Palladium. *J. Catal.* **1978**, *52*, 462–471.
61. Madon, R.J.; Oconnell, J.P.; Boudart, M. Catalytic-Hydrogenation of Cyclohexene: 2. Liquid-Phase Reaction on Supported Platinum in A Gradientless Slurry Reactor. *Aiche J.* **1978**, *24*, 904–911.
62. Segal, E.; Madon, R.J.; Boudart, M. Catalytic-Hydrogenation of Cyclohexene: 1. Vapor-Phase Reaction on Supported Platinum. *J. Catal.* **1978**, *52*, 45–49.

63. Chen, F.; Shetty, M.; Wang, M.; et al. Differences in Mechanism and Rate of Zeolite-Catalyzed Cyclohexanol Dehydration in Apolar and Aqueous Phase. *ACS Catal.* **2021**, *11*, 2879–2888.
64. He, J.Y.; Liu, M.J.; Huang, K.F.; et al. Production of levoglucosenone and 5-hydroxymethylfurfural from cellulose in polar aprotic solvent-water mixtures. *Green Chem.* **2017**, *19*, 3642–3653.
65. Qi, L.; Alamillo, R.; Elliott, W.A.; et al. Operando Solid-State NMR Observation of Solvent-Mediated Adsorption-Reaction of Carbohydrates in Zeolites. *ACS Catal.* **2017**, *7*, 3489c3500.
66. Iyemperumal, S.K.; Deskins, N.A. Evaluating Solvent Effects at the Aqueous/Pt(111) Interface. *Chemphyschem* **2017**, *18*, 2171–2190.
67. Singh, N.; Sanyal, U.; Ruehl, G.; et al. Aqueous phase catalytic and electrocatalytic hydrogenation of phenol and benzaldehyde over platinum group metals. *J. Catal.* **2020**, *382*, 372–384.
68. Xie, T.J.; Bodenschatz, C.J.; Getman, R.B. Insights into the roles of water on the aqueous phase reforming of glycerol. *React. Chem. Eng.* **2019**, *4*, 383–392.
69. Cortright, R.D.; Dumesic, J.A. Kinetics of heterogeneous catalytic reactions: Analysis of reaction schemes. *Adv. Catal.* **2001**, *46*, 161–264.
70. Dumesic, J.A. Analyses of Reaction Schemes Using De Donder relations. *J. Catal.* **1999**, *185*, 496.
71. Gokhale, A.A.; Dumesic, J.A.; Mavrikakis, M. On the mechanism of low-temperature water gas shift reaction on copper. *J. Am. Chem. Soc.* **2008**, *130*, 1402–1414.
72. Grabow, L.C.; Gokhale, A.A.; Evans, S.T.; et al. Mechanism of the water gas shift reaction on Pt: First principles, experiments, and microkinetic modeling. *J. Phys. Chem. C* **2008**, *112*, 4608–4617.
73. Kandoi, S.; Greeley, J.; Sanchez-Castillo, M.A.; et al. Prediction of experimental methanol decomposition rates on platinum from first principles. *Top. Catal.* **2006**, *37*, 17–28.
74. Motagamwala, A.H.; Dumesic, J.A. Analysis of reaction schemes using maximum rates of constituent steps. *Proc. Natl. Acad. Sci. USA* **2016**, *113*, E2879–E2888.
75. Grabow, L.C.; Mavrikakis, M. Mechanism of Methanol Synthesis on Cu through CO_2 and CO Hydrogenation. *ACS Catal.* **2011**, *1*, 365–384.
76. Motagamwala, A.H.; Dumesic, J.A. Chemical kinetics for generalized two-step reaction schemes. *J. Catal.* **2021**, *404*, 850–863.
77. Norskov, J.K.; Bligaard, T.; Logadottir, A.; et al. Universality in heterogeneous catalysis. *J. Catal.* **2002**, *209*, 275–278.
78. Ovesen, C.V.; Stoltze, P.; Norskov, J.K.; et al. A Kinetic Model of the Water-Gas Shift Reaction. *J. Catal.* **1992**, *134*, 445–468.
79. Ovesen, C.V.; Clausen, B.S.; Hammershoi, B.S.; et al. Microkinetic analysis of the water-gas shift reaction under industrial conditions. *J. Catal.* **1996**, *158*, 170–180.
80. Medford, A.J.; Vojvodic, A.; Hummelshoj, J.S.; et al. From the Sabatier principle to a predictive theory of transition-metal heterogeneous catalysis. *J. Catal.* **2015**, *328*, 36–42.
81. Moses, P.G.; Grabow, L.C.; Fernandez, E.M.; Hinnemann, B.; Topsoe, H.; Knudsen, K.G.; Norskov, J.K. Trends in Hydrodesulfurization Catalysis Based on Realistic Surface Models. *Catal. Lett.* **2014**, *144*, 1425–1432.
82. Vojvodic, A.; Norskov, J.K. New design paradigm for heterogeneous catalysts. *Natl. Sci. Rev.* **2015**, *2*, 140–143.
83. Mhadeshwar, A.B.; Vlachos, D.G. Microkinetic modeling for water-promoted CO oxidation, water-gas shift, and preferential oxidation of CO on pt. *J. Phys. Chem. B* **2004**, *108*, 15246–15258.
84. Meskine, H.; Matera, S.; Scheffler, M.; et al. Examination of the concept of degree of rate control by first-principles kinetic Monte Carlo simulations. *Surf. Sci.* **2009**, *603*, 1724–1730.
85. Reuter, K.; Frenkel, D.; Scheffler, M. The steady state of heterogeneous catalysis, studied by first-principles statistical mechanics. *Phys. Rev. Lett.* **2004**, *93*, 116105.
86. Linic, S.; Barteau, M.A. Construction of a reaction coordinate and a microkinetic model for ethylene epoxidation on silver from DFT calculations and surface science experiments. *J. Catal.* **2003**, *214*, 200–212.
87. Campbell, C.T.; Mao, Z.T. Analysis and prediction of reaction kinetics using the degree of rate control. *J. Catal.* **2021**, *404*, 647–660.
88. Mao, Z.T.; Campbell, C.T. Kinetic Isotope Effects: Interpretation and Prediction Using Degrees of Rate Control. *ACS Catal.* **2020**, *10*, 4181–4192.
89. Dix, S.T.; Scott, J.K.; Getman, R.B.; et al. Using degrees of rate control to improve selective n-butane oxidation over model MOF-encapsulated catalysts: Sterically-constrained Ag3Pd(111). *Faraday Discuss.* **2016**, *188*, 21–38.
90. Wolcott, C.A.; Medford, A.J.; Studt, F.; et al. Degree of Rate Control Approach to Computational Catalyst Screening. *J. Catal.* **2015**, *330*, 197–207.
91. Stegelmann, C.; Schiødt, N.C.; Campbell, C.T.; et al. Microkinetic modeling of ethylene oxidation over silver. *J. Catal.* **2004**, *221*, 630–649.
92. Campbell, C.T. Micro- and Macro-Kinetics: Their Relationship in Heterogeneous Catalysis. *Top. Catal.* **1994**, *1*, 353–366.

93. Bockris, J.O.M.; Jeng, K.T. In-situ studies of adsorption of organic compounds on platinum electrodes. *J. Electroanal. Chem.* **1992**, *330*, 541–581.
94. Kristoffersen, H.H.; Shea, J.-E.; Metiu, H. Catechol and HCl Adsorption on TiO_2(110) in Vacuum and at the Water–TiO_2 Interface. *J. Phys. Chem. Lett.* **2015**, *6*, 2277–2281.
95. Song, W.; Martsinovich, N.; Heckl, W.M.; et al. Born-haber cycle for monolayer self-assembly at the liquid-solid interface: Assessing the enthalpic driving force. *J. Am. Chem. Soc.* **2013**, *135*, 14854–14862.
96. Yoon, Y.; Rousseau, R.; Weber, R.S.; et al. First-Principles Study of Phenol Hydrogenation on Pt and Ni Catalysts in Aqueous Phase. *J. Am. Chem. Soc.* **2014**, *136*, 10287–10298.
97. Akinola, J.; Campbell, C.T.; Singh, N. Effects of Solvents on Adsorption Energies: A General Bond-Additivity Model. *J. Phys. Chem. C* **2021**, *125*, 24371–24380.
98. Akinola, J.; Singh, N. Temperature dependence of aqueous-phase phenol adsorption on Pt and Rh. *J. Appl. Electrochem.* **2021**, *51*, 37–50.
99. Magnussen, O.M.; Gross, A. Toward an Atomic-Scale Understanding of Electrochemical Interface Structure and Dynamics. *J. Am. Chem. Soc.* **2019**, *141*, 4777–4790.
100. Singh, N.; Lee, M.S.; Akhade, S.A.; et al. Impact of pH on Aqueous-Phase Phenol Hydrogenation Catalyzed by Carbon-Supported Pt and Rh. *ACS Catal.* **2019**, *9*, 1120–1128.
101. Saleheen, M.; Heyden, A. Liquid-Phase Modeling in Heterogeneous Catalysis. *ACS Catal.* **2018**, *8*, 2188–2194.
102. Zhang, X.H.; Sewell, T.E.; Glatz, B.; et al. On the water structure at hydrophobic interfaces and the roles of water on transition-metal catalyzed reactions: A short review. *Catal. Today* **2017**, *285*, 57–64.
103. Zhang, X.H.; DeFever, R.S.; Sarupria, S.; et al. Free Energies of Catalytic Species Adsorbed to Pt(111) Surfaces under Liquid Solvent Calculated Using Classical and Quantum Approaches. *J. Chem. Inf. Model.* **2019**, *59*, 2190–2198.
104. Granda-Marulanda, L.P.; Builes, S.; Koper, M.T.M.; et al. Influence of Van der Waals Interactions on the Solvation Energies of Adsorbates at Pt-Based Electrocatalysts. *Chemphyschem* **2019**, *20*, 2968–2972. https://doi.org/10.1002/cphc.201900512.
105. Gray, C.M.; Saravanan, K.; Wang, G.F.; et al. Quantifying solvation energies at solid/liquid interfaces using continuum solvation methods. *Mol. Simul.* **2017**, *43*, 420–427.
106. Clabaut, P.; Schweitzer, B.; Götz, A.W.; et al. Solvation Free Energies and Adsorption Energies at the Metal/Water Interface from Hybrid Quantum-Mechanical/Molecular Mechanics Simulations. *J. Chem. Theory Comput.* **2020**, *16*, 6539–6549.
107. Gu, G.H.; Schweitzer, B.; Michel, C.; et al. Group Additivity for Aqueous Phase Thermochemical Properties of Alcohols on Pt(111). *J. Phys. Chem. C* **2017**, *121*, 21510–21519.
108. Klamt, A.; Schuurmann, G. Cosmo–A New Approach to Dielectric Screening in Solvents with Explicit Expressions for The Screening Energy and Its Gradient. *J. Chem. Soc. Perkin Trans.* **1993**, *2*, 799–805.
109. Schweitzer, B.; Steinmann, S.N.; Michel, C. Can microsolvation effects be estimated from vacuum computations? A case-study of alcohol decomposition at the H_2O/Pt(111) interface. *Phys. Chem. Chem. Phys.* **2019**, *21*, 5368–5377.
110. Yuk, S.F.; Lee, M.S.; Akhade, S.A.; et al. First-principle investigation on catalytic hydrogenation of benzaldehyde over Pt-group metals. *Catal. Today* **2022**, *388*, 208–215.
111. Zhang, X.H.; Savara, A.; Getman, R.B. A Method for Obtaining Liquid-Solid Adsorption Rates from Molecular Dynamics Simulations: Applied to Methanol on Pt(111) in H_2O. *J. Chem. Theory Comput.* **2020**, *16*, 2680–2691.
112. Zare, M.; Solomon, R.V.; Yang, W.Q.; et al. Theoretical Investigation of Solvent Effects on the Hydrodeoxygenation of Propionic Acid over a Ni(111) Catalyst Model. *J. Phys. Chem. C* **2020**, *124*, 16488–16500.
113. Fiorentin, M.R.; Bianchi, M.G.; Christiansen, M.A.H.; et al. Methodological Frameworks for Computational Electrocatalysis: From Theory to Practice. *Small Methods* **2026**, *10*, e01542.
114. Chukwu, K.C.; Arnadóttir, L. Effects of co-adsorbed water on different bond cleavages involved in acetic acid decomposition on Pt(111). *Surf. Sci.* **2025**, *756*, 122721.
115. Hanselman, S.; Koper, M.T.M.; Calle-Vallejo, F. Using micro-solvation and generalized coordination numbers to estimate the solvation energies of adsorbed hydroxyl on metal nanoparticles. *Phys. Chem. Chem. Phys.* **2023**, *25*, 3211–3219.
116. Heenen, H.H.; Gauthier, J.A.; Kristoffersen, H.H.; et al. Solvation at metal/water interfaces: An ab initio molecular dynamics benchmark of common computational approaches. *J. Chem. Phys.* **2020**, *152*, 144703.
117. Baricuatro, J.H.; Kwon, S.; Kim, Y.G.; et al. Operando Electrochemical Spectroscopy for CO on Cu(100) at pH 1 to 13: Validation of Grand Canonical Potential Predictions. *ACS Catal.* **2021**, *11*, 3173–3181.
118. Hussain, J.; Jónsson, H.; Skúlason, E. Calculations of Product Selectivity in Electrochemical CO2 Reduction. *Acs Catal.* **2018**, *8*, 5240–5249.
119. Skúlason, E.; Bligaard, T.; Gudmundsdóttir, S.; et al. A theoretical evaluation of possible transition metal electro-catalysts for N2 reduction. *Phys. Chem. Chem. Phys.* **2012**, *14*, 1235–1245.

120. Barth, I.; Akinola, J.; Lee, J.; et al. Explaining the structure sensitivity of Pt and Rh for aqueous-phase hydrogenation of phenol. *J. Chem. Phys.* **2022**, *156*, 104703.
121. Baghdady, E.A.; Medlin, J.W.; Schwartz, D.K. Tuning formate surface coverage with cosolvents for liquid-phase catalytic transfer hydrogenation. *Catal. Sci. Technol.* **2025**, *15*, 3354–3362.
122. Rumptz, J.R.; Campbell, C.T. Adhesion Energies of Solvent Films to Pt(111) and Ni(111) Surfaces by Adsorption Calorimetry. *ACS Catal.* **2019**, *9*, 11819–11825.
123. Rumptz, J.R.; Campbell, C.T. Adhesion Energies of Liquid Hydrocarbon Solvents onto Pt(111), MgO(100), Graphene, and TiO_2(110) from Temperature-Programmed Desorption Energies. *J. Phys. Chem. C* **2021**, *125*, 27931–27937.
124. Mallat, T.; Baiker, A. Catalyst potential measurement: A valuable tool for understanding and controlling liquid phase redox reactions. *Top. Catal.* **1999**, *8*, 115–124.
125. Adams, J.S.; Kromer, M.L.; Rodríguez-López, J.; Flaherty, D.W. Unifying Concepts in Electro- and Thermocatalysis toward Hydrogen Peroxide Production. *J. Am. Chem. Soc.* **2021**, *143*, 7940–7957.
126. Ryu, J.; Bregante, D.T.; Howland, W.C.; et al. Thermochemical aerobic oxidation catalysis in water can be analysed as two coupled electrochemical half-reactions. *Nat. Catal.* **2021**, *4*, 742–752.
127. Wesley, T.S.; Román-Leshkov, Y.; Surendranath, Y. Spontaneous Electric Fields Play a Key Role in Thermochemical Catalysis at Metal-Liquid Interfaces. *ACS Cent. Sci.* **2021**, *7*, 1045–1055.
128. Howland, W.C.; Gerken, J.B.; Stahl, S.S.; et al. Thermal Hydroquinone Oxidation on Co/N-doped Carbon Proceeds by a Band-Mediated Electrochemical Mechanism. *J. Am. Chem. Soc.* **2022**, *144*, 11253–11262.
129. Fortunato, G.V.; Pizzutilo, E.; Katsounaros, I.; et al. Analysing the relationship between the fields of thermo- and electrocatalysis taking hydrogen peroxide as a case study. *Nat. Commun.* **2022**, *13*, 1973.
130. Lodaya, K.M.; Tang, B.Y.; Bisbey, R.P.; et al. An electrochemical approach for designing thermochemical bimetallic nitrate hydrogenation catalysts. *Nat. Catal.* **2024**, *7*, 262–272.
131. Westendorff, K.S.; Hülsey, M.J.; Wesley, T.S.; et al. Electrically driven proton transfer promotes Brønsted acid catalysis by orders of magnitude. *Science* **2024**, *383*, 757–763.
132. Razdan, N.K.; Westendorff, K.S.; Surendranath, Y. Wireless potentiometry of thermochemical heterogeneous catalysis. *Nat. Catal.* **2025**, *8*, 315–327.
133. Harraz, D.M.; Lodaya, K.M.; Tang, B.Y.; et al. Homogeneous-heterogeneous bifunctionality in Pd-catalyzed vinyl acetate synthesis. *Science* **2025**, *388*, eads7913.
134. Campbell, C.T. Effects of Electric Fields on the Energies of Adsorbates on Metal Surfaces in Vacuum and in Liquids. *ACS Catal.* **2026**, *16*, 5294–5308.
135. Sheng, W.C.; Zhuang, Z.B.; Gao, M.R.; et al. Correlating hydrogen oxidation and evolution activity on platinum at different pH with measured hydrogen binding energy. *Nat. Commun.* **2015**, *6*, 5848.
136. McGregor, J.M.; Bender, J.T.; Petersen, A.S.; et al. Organic electrolyte cations promote non-aqueous CO2 reduction by mediating interfacial electric fields. *Nat. Catal.* **2025**, *8*, 79–91.